NANO LETTERS

2005
Vol. 5, No. 4
609−613

Electrochemical Nanofabrication Using Crystalline Protein Masks

Daniel B. Allred,[†] Mehmet Sarikaya,[†,‡] François Baneyx,[†] and Daniel T. Schwartz*[,†,‡]

Chemical Engineering Department and Materials Science and Engineering Department, University of Washington, Seattle, Washington 98195-1750

Received December 8, 2004

ABSTRACT

We have developed a simple and robust method to fabricate nanoarrays of metals and metal oxides over macroscopic substrates using the crystalline surface layer (S-layer) protein of *Deinococcus radiodurans* as an electrodeposition mask. Substrates are coated by adsorption of the S-layer from a detergent-stabilized aqueous protein extract, producing insulating masks with 2–3 nm diameter solvent-accessible openings to the deposition substrate. The coating process can be controlled to achieve complete or fractional surface coverage. We demonstrate the general applicability of the technique by forming arrays of cuprous oxide (Cu_2O), Ni, Pt, Pd, and Co exhibiting long-range order with the 18 nm hexagonal periodicity of the protein openings. This protein-based approach to electrochemical nanofabrication should permit the creation of a wide variety of two-dimensional inorganic structures.

Through-mask electrodeposition has been used extensively to pattern metals, semiconductors, and polymers on conductive substrates.[1−4] The mask, a patterned arrangement of solvent-accessible openings, limits the regions of the substrate where material growth occurs, thereby allowing synthesis of a high fidelity negative replica with nanometer-thickness control.[5] Emerging techniques for electrochemical nanofabrication frequently exploit masks that self-organize, such as anodic alumina[6−14] and molecular crystals such as amphiphilic surfactants[15−18] and block-copolymers.[19] Unfortunately, these self-assembling masks form a limited number of unit cell geometries, precluding the creation of complex patterns. Proteins can organize into homo- or heterostructures representing all possible two-dimensional (2-D) space groups built from chiral molecules. Moreover, they are readily engineered through molecular biology, providing an attractive foundation for nanotechnology. As a result, crystalline protein architectures have been used as templates for organizing nanoparticle arrays,[20−23] as shadow masks for nanoarray synthesis via vapor-phase deposition,[24−28] and many other nanofabrication approaches.

To the best of our knowledge, electrodeposition through crystalline protein masks has not been demonstrated as a robust nanofabrication strategy. In electrodeposition, material growth proceeds from the substrate outward and need not follow a line-of-sight path through the mask (as do many vapor-phase deposition methods). Thus, electrodeposition offers the unique prospect of being able to grow dense materials through a tortuous multilayer crystalline protein mask, or other complex protein structure, thereby relaxing the difficult task of optimizing the protein−surface interface[29] to attain perfect monolayer coverage.

Of particular interest for bio-inspired nanofabrication are surface layer (S-layer) proteins, a class of 2-D crystalline proteins that encapsulate certain bacterial cells, protecting them from extracellular enzymes and regulating molecular trafficking.[30] S-layers are highly resistant to conditions that normally denature proteins (e.g., low pH, chaotropic agents, and heat)[31] and can assemble into all 2-D rotational symmetries (p1, p2, p3, p4, and p6). They have 1−4 nm solvent-accessible openings organized with typical lattice parameters ranging from 10 to 20 nm.[32] To demonstrate the potential of S-layer proteins for through-mask electrodeposition, we selected the hexagonally packed intermediate (HPI) layer from *Deinococcus radiodurans* based on its chemical resistance[33,34] and ease of purification in the crystalline state.[35,36] The HPI layer is tethered to the bacterium via hydrophobic interactions that are disrupted upon detergent addition. Indeed, incubation of the cells with 5% sodium dodecyl sulfate (SDS) at 60 °C for 2 h caused large crystalline protein sheets to slough from the cell surface, as imaged in Figure 1 using glutaraldehyde-fixed, uranyl acetate-stained samples. Higher magnification imaging (inset) confirmed the expected structure of the HPI layer, a hexagonal array (p6, 18 nm) of hexameric proteins pierced with 2−3 nm pores.[37] Purification of the HPI layer protein was accomplished by repeated centrifugation, decanting, and

* Corresponding author. E-mail: dts@u.washington.edu.
[†] Chemical Engineering Department.
[‡] Materials Science and Engineering Department.

10.1021/nl047967b CCC: $30.25
Published on Web 01/28/2005

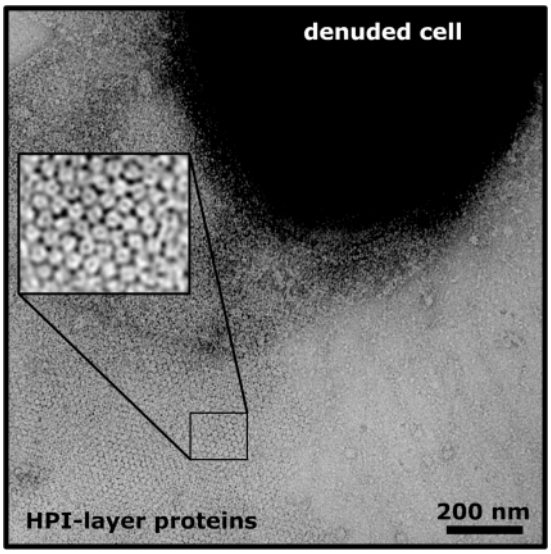

Figure 1. TEM image of glutaraldehyde-fixed and uranyl acetate-stained *Deinococcus radiodurans* after detergent treatment. A portion of the cell and the partially sloughed HPI layer proteins are labeled. Inset: higher magnification image of the HPI layer proteins shown in the smaller window.

pellet resuspension in 5% SDS.[38] Purified HPI layer proteins were stored at room temperature in 0.1−1 mg mL^{-1} stock solutions in 5% SDS. Imaging with transmission electron microscopy (TEM) and atomic force microscopy (AFM),[39] as well as electrophoresis experiments, revealed that protein solutions can be stored for at least 6 months in 5% SDS at room temperature without loss of crystalline order or proteolytic degradation.

In most cases examined, proteins were partially coated on substrates to compare material nucleation and growth on adjacent protein-covered and bare regions.[40] Typical surface coverages were 40% to 80%, corresponding to roughly 2−60 min of substrate contact time with the stock protein solution. AFM examination of partially covered surfaces (Figure 2A) shows that protein monolayers are 5−6 nm in height with single-crystal domain sizes around 1 μm. Additional features are evident, such as protein crystals that have folded onto themselves. Higher resolution imaging (Figure 2A, inset) reveals the presence of two different types of putative protein openings, one or both of which must be solvent accessible for *D. radiodurans* to live. Complete surface coverage was achieved by multilayer adsorption of HPI layer protein crystals, leading to the more pronounced surface topography seen in Figure 2B.

The substrates used for electrodeposition studies were ultrathin AuPd films draped across the imaging windows of gold TEM specimen grids.[41] These electron-transparent films permitted high quality electrodeposition, TEM imaging, and electron diffraction-based characterization. Potentiostatic electrodeposition of cuprous oxide (Cu_2O) from a room temperature, pH 9, 0.4 M $CuSO_4$, 3 M lactic acid bath produced well-nucleated films on the bare TEM grid substrates.[42] Figure 3A shows that Cu_2O grown on substrates partially covered with proteins produced 0.5 to 1 μm patches displaying the 18-nm hexagonal periodicity of the protein,

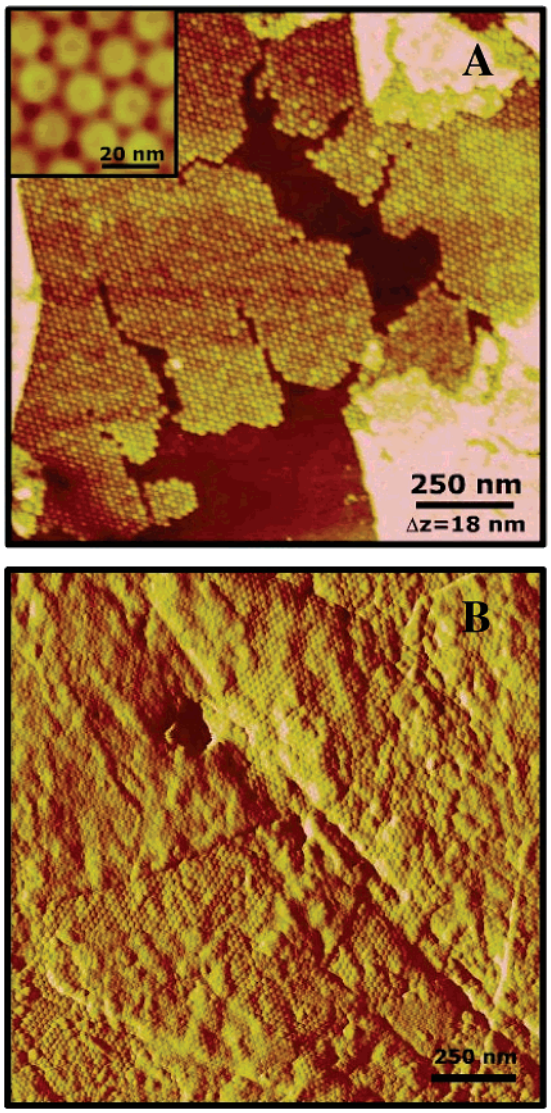

Figure 2. (A) Tapping mode AFM image of HPI layer proteins on a polished steel disk reveals typical coverage when proteins are contacted for several minutes before washing. Inset: higher resolution image on freshly cleaved mica revealed patterned arrangement of channels. (B) Tapping mode AFM image of HPI-layer proteins completely covering a polished gold foil. Image is shown in deflection mode due to the pronounced topography of the height mode.

along with regions of plain film typical of growth on the bare substrate. The protein itself is transparent in the TEM under the imaging conditions (120 kV accelerating voltage), so the observed hexagonal structure is due to electrodeposited inorganic masked by the protein. Fast Fourier transform (FFT) analysis of Figure 3A confirms that the deposit has long-range order with 18 nm periodicity (upper left inset). The higher resolution Fourier-filtered image (upper right inset) suggests that each of the two putative protein openings seen in Figure 2A can be filled by electrodeposition, though perhaps not equally well. Figure 3B shows a cross-sectional schematic illustration of the through-protein deposition process in the protein-covered and bare substrate regions.

Results from electron diffraction studies (Figure 3C) confirm that the electrodeposited inorganic is Cu_2O in both

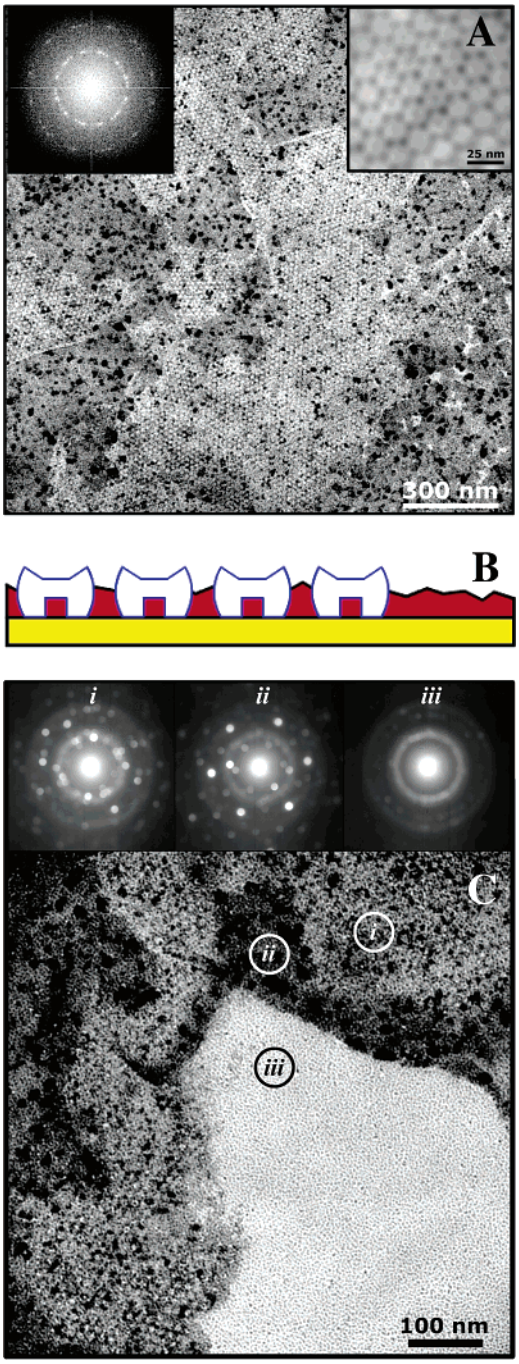

Figure 3. TEM imaging and electron diffraction of Cu_2O electrodeposited under partial protein coverage conditions. (A) Low magnification image of a typical Cu_2O film electrodeposited on a thin film substrate partially coated with HPI layer proteins. FFT analysis (left inset) reveals a mosaic of variously rotated structures with 18-nm hexagonal periodicity. FFT-filtered image (right inset) shows excellent fidelity of the electrodeposited material to the protein structure. (B) Schematic cross-section of the proposed deposit. (C) An areaof film showing nanostructured Cu_2O (*i*), unpatterned Cu_2O (*ii*), and bare substrate (*iii*). Electron diffraction patterns from a ~50 nm probe are shown along the top. Weak Au−Pd background diffraction is seen in all three regions, but does not obscure the strong pattern from the Cu_2O cuprite structure of the electrodeposited film in regions (*i*) and (*ii*).

the protein-covered region and on the bare substrate. The image shows a portion of the substrate with three distinct regions. Diffraction from region (i), an area where protein-masked electrodeposition is visible, has the cuprite structure of Cu_2O ($Pn3m-O_h^4$) superimposed on the AuPd substrate diffraction. Region (ii), an area where deposition occurred on unmasked AuPd substrate, also exhibits a cuprite crystal structure. Finally, region (iii) is bare AuPd substrate showing the weak, broad background diffraction from the 1−2 nm grains of the ultrathin AuPd substrate. Electron diffraction over larger areas (not shown) further confirms that all electron-dense regions are primarily composed of polycrystalline Cu_2O. Thus, the protein mask has not significantly modified the material produced by the electrodeposition process.

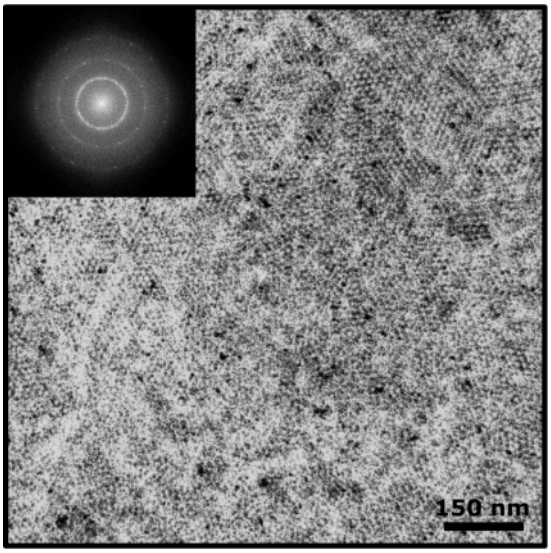

Figure 4. TEM image of Cu_2O electrodeposited through multilayer protein with complete surface coverage. Inset: Computed FFT of the low-resolution image.

Electrodeposition on substrates that were completely covered with multilayers of S-layer proteins produced hexagonal arrays of Cu_2O over the entire observable surface of the 3 mm-diameter thin film substrate (typical region shown in Figure 4). The intense rings seen in the FFT inset indicate that the electrodeposited structure exhibits the long-range periodicity of the protein, but is a mosaic of many rotated protein crystals. We also observed various local Moiré patterns, likely resulting from material growth through more than one protein layer. Thus, electrodeposition can readily proceed through multilayer protein films, demonstrating its value as a material growth strategy vis-à-vis a line-of-sight deposition method.

To demonstrate the generality of the above strategy with other materials, nickel, platinum, palladium, and cobalt were electrodeposited on TEM substrates with partial HPI layer protein coverage. These systems represent a wide range of electrolyte characteristics, as noted below. Despite having done little optimization of the electrodeposition conditions for each metal, ordered nanostructures were seen in all cases (see Figure 5 and insets). FFT analysis confirmed that electrodeposition occurred through the protein mask (see left insets). The density of openings in the HPI-layer mask demands nucleation densities on the substrate of $\sim 10^{12}$ cm^{-2} to completely and uniformly fill the mask. The room

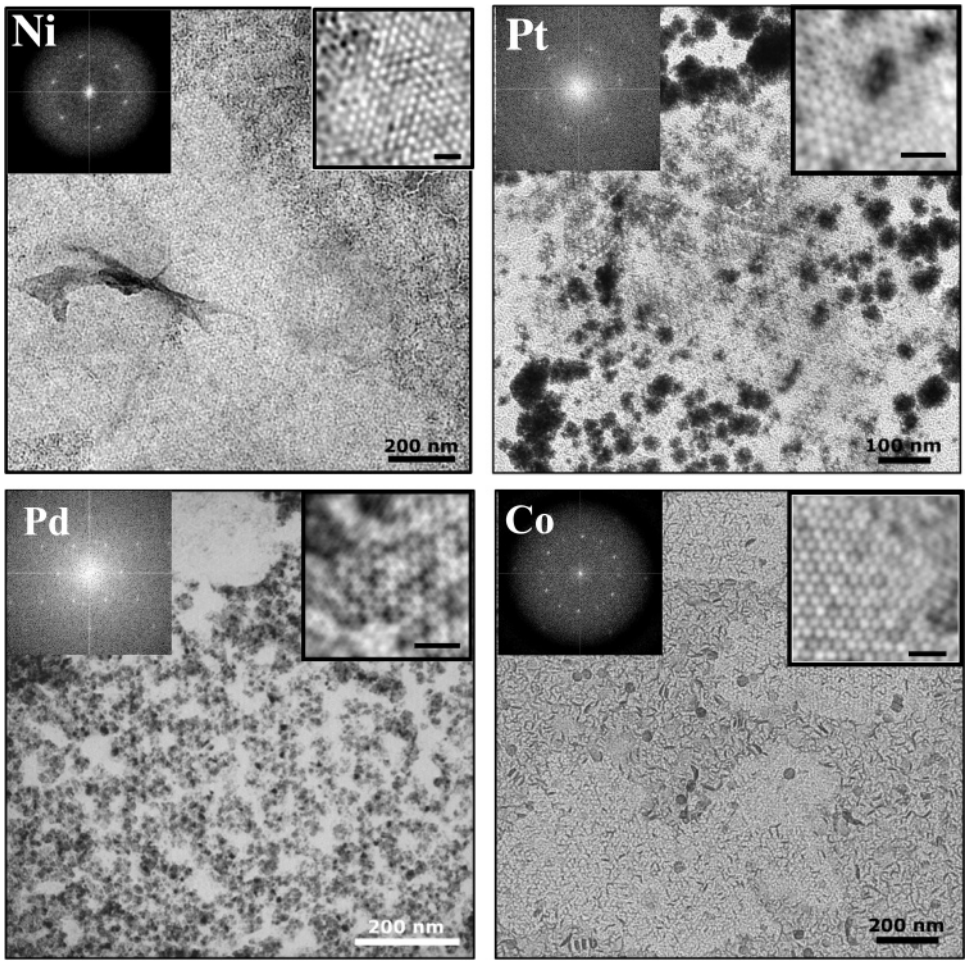

Figure 5. TEM images of nickel, platinum, palladium, and cobalt electrodeposited through HPI layers under partial protein coverage conditions. Each image has an FFT-filtered inset of the deposit (size bar = 40 nm) and a computed FFT inset showing long-range order.

temperature potentiostatic deposition of Pt and Pd (from the commercial baths Platinum AP and Pallaspeed by Technics) clearly did not fully nucleate, producing patchy deposits. The potentiostatic growth of Co and Ni (from an ethanol-based electrolyte and a Watts-type electrolyte, respectively) developed strong crystalline texture with characteristic dimensions larger than the periodicity of the protein or the crystalline grain size of the substrate. These results show that optimization of the mask filling process requires careful attention to nucleation densities on the substrate. A comparison between masked and unmasked regions on each substrate suggests that the protein did not substantially change the character of nucleation. Hence, unmasked substrates can probably be used to optimize the nucleation and growth processes of a particular material of interest (via pulse plating, applied potential, and/or use of surface active agents), as is typical in electrodeposition research. Once optimal growth conditions are found, full protein coverage conditions can be used for the routine preparation of nanostructured surfaces, as demonstrated for the case of Cu_2O. The wide range and nature of the electrolytes used here highlights the stability of this S-layer protein to chemical environment.

In summary, we have shown that electrodeposition through the crystalline *D. radiodurans* HPI-layer is a reliable and easily implemented technique for the fabrication of a variety of nanostructured materials on electrically conducting substrates. Because the stacking of multiple HPI layer protein crystals does not stop the material growth processes, patterning over millimeter distances is possible using crystalline arrays isolated directly from the cell without the difficult task of reassembling individual subunits into large single monolayer crystals. On the other hand, careful control of the deposition thickness and nucleation properties are necessary to achieve uniform surfaces due to the small opening sizes and dense lateral spacing. The *D. radiodurans* HPI layer is a robust protein that remains structurally intact under a wide range of environmental conditions. Because this characteristic is shared by many class members, S-layer proteins from other organisms, and possibly other self-assembling proteins, will certainly prove useful for the electrodeposition of ordered nanostructures with a variety of superlattice symmetries.

Acknowledgment. D.A. is grateful to Phil Bartlett, Mamdouh Abdelsalem, and Stuart Evans at the University of Southampton, UK for the opportunity to learn templated electrodeposition via a Worldwide Universities Network Global Exchange Fellowship (WUN). We thank Haixia Dai, Hanson Fong, Thurston Herricks, and Tom Murray for valuable recommendations and suggestions. This work was

supported by the U.S. Army Research Office-Defense University Research Initiative in NanoTechnology (ARO-DURINT: DAAD19-01-1-04999), the National Science Foundation-Integrative Graduate Education Research Traineeship (NSF-IGERT) in Nanotechnology, and the Boeing-Sutter Endowment.

References

(1) Romankiw, L. T. *Electrochim. Acta* **1997**, *42*, 2985.
(2) Andricacos, P. C.; Uzoh, C.; Dukovic, J. O.; Horkans, J.; Deligianni, H. *IBM J. Res. Dev.* **1998**, *42*, 567.
(3) Datta, M. *Electrochim. Acta* **2003**, *48*, 2975.
(4) Datta, M.; Landolt, D. *Electrochim. Acta* **2000**, *45*, 2535.
(5) Schwarzacher, W.; Kasyutich, O. I.; Evans, P. R.; Darbyshire, M. G.; Yi, G.; Fedosyuk, V. M.; Rousseaux, F.; Cambril, E.; Decanini, D. *J. Magn. Magn. Mater.* **1999**, *198*−*199*, 185.
(6) Al-Mawlawi, D.; Liu, C. Z.; Moskovits, M. *J. Mater. Res.* **1994**, *9*, 1014.
(7) Zangari, G.; Lambeth, D. N. *IEEE Trans. Magn.* **1997**, *33*, 3010.
(8) Chu, S.-Z.; Wada, K.; Inoue, S.; Todoroki, S.-i. *Chem. Mater.* **2002**, *14*, 4595.
(9) Sander, M. S.; Prieto, A. L.; Gronsky, R.; Sands, T.; Stacy, A. M. *Adv. Mater.* **2002**, *14*, 665.
(10) Kolmakov, A.; Zhang, Y.; Cheng, G.; Moskovits, M. *Adv. Mater.* **2003**, *15*, 997.
(11) Nicewarner-Peña, S. R.; Carado, A. J.; Shale, K. E.; Keating, C. D. *J. Phys. Chem. B* **2003**, *107*, 7360.
(12) Ohgai, T.; Gravier, L.; Hoffer, X.; Lindeberg, M.; Hjort, K.; Spohr, R.; Ansermet, J.-P. *J. Phys. D: Appl. Phys.* **2003**, *36*, 3109.
(13) Knaack, S. A.; Eddington, J.; Leonard, Q.; Cerrina, F.; Onellion, M. *Appl. Phys. Lett.* **2004**, *84*, 3388.
(14) Oh, J.; Tak, Y.; Lee, J. *Electrochem. Solid State* **2004**, *7*, C27.
(15) Attard, G. S.; Bartlett, P. N.; Coleman, N. R. B.; Elliott, J. M.; Owen, J. R.; Wang, J. H. *Science* **1997**, *278*, 838.
(16) Bartlett, P. N.; Birkin, P. N.; Ghanem, M. A.; de Groot, P.; Sawicki, M. *J. Electrochem. Soc.* **2001**, *148*, C119.
(17) Huang, L.; Wang, H.; Wang, Z.; Mitra, A.; Zhao, D.; Yan, Y. *Chem. Mater.* **2002**, *14*, 876.
(18) Zhao, J. K.; Chen, X.; Jiao, L. Y.; Chai, Y. c.; Zhang, G. D.; Liu, J. *Chem. Lett.* **2004**, *33*, 842.
(19) Thurn-Albrecht, T.; Schotter, J.; Kästle, G. A.; Emley, N.; Shibauchi, T.; Krusin-Elbaum, L.; Guarini, K.; Black, C. T.; Tuominen, M. T.; Russell, T. P. *Science* **2000**, *290*, 2126.
(20) Shenton, W.; Pum, D.; Sleytr, U. B.; Mann, S. *Nature* **1997**, *389*, 585.
(21) Mertig, M.; Kirsch, R.; Pompe, W.; Engelhardt, H. *Eur. Phys. J. D* **1999**, *9*, 45.
(22) Hall, S. R.; Shenton, W.; Engelhardt, H.; Mann, S. *Chem. Phys. Chem.* **2001**, 184.
(23) McMillan, R. A.; Paavola, C. D.; Howard, J.; Chan, S. L.; Zaluzec, N. J.; Trent, J. D. *Nature Mater.* **2002**, *1*, 247.
(24) Douglas, K.; Devaud, G.; Clark, N. A. *Science* **1992**, *257*, 642.
(25) Moore, J. T.; Beale, P. D.; Winningam, T. A.; Douglas, K. *Appl. Phys. Lett.* **1997**, *71*, 1264.
(26) Moore, J. T.; Beale, P. D.; Winningham, T. A.; Douglas, K. *Appl. Phys. Lett.* **1998**, *72*, 1840.
(27) Panhorst, M.; Brückl, H.; Kiefer, B.; Reiss, G.; Santarius, U.; Guckenberger, R. *J. Vac. Sci. Technol. B* **2001**, *19*, 722.
(28) Malkinski, L.; Camley, R. E.; Celinski, Z.; Winningham, T. A.; Whipple, S. G.; Douglas, K. *J. Appl. Phys.* **2003**, *93*, 7325.
(29) Pum, D.; Sleytr, U. B. *Supramol. Sci.* **1995**, *2*, 193.
(30) Sleytr, U. B.; Schuster, B.; Pum, D. *IEEE Eng. Med. Biol.* **2003**, *22*, 140.
(31) Engelhardt, H.; Peters, J. *J. Struct. Biol.* **1998**, *124*, 276.
(32) Sleytr, U. B.; Messner, P.; Pum, D.; Sára, M. *Crystalline bacterial cell surface proteins*; Academic Press: Austin, Texas, 1996.
(33) Lancy, P., Jr.; Murray, R. G. E. *Can. J. Microbiol.* **1978**, *24*, 162.
(34) Thompson, B. G.; Murray, R. G. E.; Boyce, J. F. *Can. J. Microbiol.* **1982**, *28*, 1081.
(35) Baumeister, W.; Kübler, O.; Zingsheim, H. P. *J. Ultrastruct. Res.* **1981**, *75*, 60.
(36) Baumeister, W.; Karrenberg, F.; Rachel, R.; Engel, A.; Ten Heggeler, B.; Saxton, W. O. *Eur. J. Biochem.* **1982**, *125*, 535.
(37) Rachel, R.; Jakubowski, U.; Tietz, H.; Hegerl, R.; Baumeister, W. *Ultramicroscopy* **1986**, *20*, 305.
(38) The hexagonally packed intermediate (HPI) layer protein was purified by adapting published methods.[35] Briefly, *Deinococcus radiodurans* (ATTC 35073) was grown in 1 L shake flasks in TGY medium (0.5% tryptone, 0.3% yeast extract, 0.1% glucose) at 30 °C to early stationary phase. Cells were sedimented at 2200 g for 5 min, washed twice with ddH_2O and resuspended in 5% SDS. The suspension was incubated at 60 °C with shaking for 2 h to release HPI layer proteins. Denuded cells were twice sedimented by centrifugation at 2200 g for 15 min and discarded. HPI layer proteins were obtained by centrifuging the supernatant at 18 000 g for 45 min and resuspending in 5% SDS. Typical protein yield was 2 to 3 mg L^{-1}, which is sufficient to completely mask ∼100 cm^2 of substrate with excess multilayer coverage. Purified HPI layer proteins were stored at room temperature in 0.1−1 mg mL^{-1} stock solutions in 5% SDS.
(39) For cells and protein TEM imaging, 2−5 μL of cellular suspension after detergent treatment was applied on a carbon-coated TEM grid (SPI Supplies). The samples were fixed in 2.5% glutaraldehyde for 5 min, rinsed, stained with 2% uranyl acetate for 2 min, rinsed again, and dried under vacuum. Electrodeposited films on metal-coated TEM grids required no further preparation. TEM images were obtained with a Phillips 420 TEM (C_s ∼ 1.3 mm) operated at 120 kV accelerating voltage and a 20 μm objective aperture. Samples were placed on a single-tilt specimen holder in contact with a liquid nitrogen decontamination trap. Electron diffraction was performed with a 50-nm electron probe, and the effective camera length was calibrated with an aluminum foil standard. For AFM imaging, proteins were coated on a polished steel disk or on freshly cleaved mica. Tapping mode AFM images were obtained on a Nanoscope III AFM using ∼300 kHz cantilevers with 10-nm nominal radius tips (Molecular Imaging) at a scan rate of 0.6−1.2 Hz under ambient conditions.
(40) About 20−40 μL cm^{-2} of stock HPI layer solution (0.1−1 mg mL^{-1}) was applied onto the surface by pipet. For partial coverage, the protein suspension was wicked away after 2−60 min (∼40−80% coverage) with a laboratory tissue and the surface was repeatedly rinsed by immersion in ddH_2O then allowed to air dry. For complete coverage, the protein suspension was allowed to air dry first, after which the surface was repeatedly immersed in ddH_2O followed by air drying.
(41) Substrates for TEM imaging were ultrathin films of $Au_{60}Pd_{40}$ alloy made by Ar^+ sputtering an appropriate target disk for 10−20 s using a sputter coater (SPI Supplies) operated at 100 mTorr with a plasma current of 0.75 mA/cm^2. The films were sputtered onto ink-coated microscope slides, floated off in methanol, and picked up on gold TEM grids (SPI Supplies). Metal-coated TEM grids made in this manner had adequate electron transmission properties for high-resolution imaging and outstanding properties for high nucleation density electrodeposition.
(42) All electrodeposition experiments were conducted at 23 °C using a PAR 273 potentiostat and a quiescent 10 mL single compartment cell, with a platinum counter electrode and saturated calomel electrode (SCE) or platinum wire (for cobalt plating) as reference. Electrolyte solutions were prepared from reagent grade chemicals (Sigma and Alfa Aesar) and passed through 0.2-μm filters (Osmonics, Inc.) before use. Cu_2O electrodeposition was performed at −450 mV vs SCE for 15 min using 0.4 M $CuSO_4$, 3 M lactic acid, adjusted to pH 9.0 with NaOH.[43,44] Cobalt was electrodeposited from 0.1 M $CoCl_2$ in ethanol at −1700 mV vs Pt pseudo-reference for 2 min.[45] Nickel was electrodeposited from a Watts type bath, 1 M $NiSO_4$, 0.2 M $NiCl_2$, 0.5 M boric acid at −750 mV vs SCE for 1 min. Platinum electrodeposition from a dinitrosulphatoplatinous acid bath [$H_2Pt(NO_2)_2SO_4$], (Technics Platinum AP) was performed at −175 mV vs SCE for 2 min, while palladium electrodeposition from a palladium chloride bath (Technics Pallaspeed) was performed at −900 mV vs SCE for 2 min. Deposition on the protein-coated side of the TEM substrate was assured by limiting the contact of the electrolyte meniscus to that side.
(43) Stareck, J. E., U.S. Patent 2,081,121; 1937.
(44) Golden, T. D.; Shumsky, M. G.; Zhou, Y.; VanderWerf, R. A.; Van Leeuwen, R. A.; Switzer, J. A. *Chem. Mater.* **1996**, *8*, 2499.
(45) Suzuki, A.; Watanabe, T. *J. Japan Inst. Met.* **2000**, *64*, 869.

NL047967B